



Carbon cloth-based immunosensor for detection of 25-hydroxy vitamin D₃

Deepika Chauhan¹ · Amit K. Yadav¹ · Pratima R. Solanki¹

Received: 23 November 2020 / Accepted: 8 February 2021 / Published online: 1 April 2021
© The Author(s), under exclusive licence to Springer-Verlag GmbH Austria, part of Springer Nature 2021

Abstract

Vitamin D (VD) deficiency is a global health concern due to its serious health impacts, and at present, the monitoring of VD status is expensive. Here, a novel immunosensor for sensitive and label-free detection of 25-hydroxy vitamin D₃ (25VD₃) is reported. Nanostructured cerium(IV) oxide (nCeO₂) was anchored onto carbon cloth (CC) via electrophoretic deposition to fabricate a nanoplatform (nCeO₂/CC). Subsequently, bioactive molecules (anti-25VD₃ and BSA) were introduced to fabricate the nanobioplatform BSA/anti-25VD₃/nCeO₂/CC as an immunosensor. The analytical performance of the developed immunosensor was studied towards 25VD₃ detection. The immunosensor provides a broad linear range of 1–200 ng mL⁻¹, high sensitivity of 2.08 μA ng⁻¹ mL cm⁻², a detection limit of 4.63 ng mL⁻¹, and a response time of 15 min, which is better than that of previous reports. The biosensor exhibited high selectivity, good reproducibility, and excellent stability for about 45 days. The potential application of the proposed immunosensor was observed for real serum samples towards 25VD₃ detection that demonstrated a high correlation with the conventional enzyme-linked immunosorbent assay.

Keywords Carbon cloth · Nanostructured ceria · Immunosensor · 25-Hydroxy vitamin D₃ · Serum sample

Introduction

Vitamin D (VD) deficiency is a global health concern due to its serious health impacts including bone disorder, cardiovascular diseases, infections, diabetes, osteoarthritis, tuberculosis, hypertension, and even cancer. Besides this, there are many other physiological functions in which VD endocrine system helps to modulate and they have a direct relation with VD, viz immune response, regulation of cell proliferation, and differentiation [1, 2]. Recently, scientists have also correlated VD deficiency with the COVID-19 cases. Various reports showed a correlation between VD deficiency and risk of COVID-19. The study also showed that peoples having lower VD level developed more inflammatory markers (ferritin and D-dimer) that are linked to poor COVID-19 outcomes. It has been reported that VD might be helpful to prevent “cytokine storms” seen in few COVID-19 patients by attenuating the immune system response. Also, supplementation of VD₃ could be a

promising approach to reduce the risk of COVID-19 [weblink 1, weblink 2, weblink 3, and weblink 4]. VD is available in two major forms, namely VD₂ and VD₃, and the available research reports suggest the preferable form is VD₃ over VD₂. Further, out of all the available analytical forms of VD₃, clinical research considered 25-hydroxy vitamin D₃ (25VD₃) as the best parameter to indicate VD status. It is due to the reason that 25VD₃ has a much higher serum concentration (~ 99%) and a longer half-life (about 3 weeks) and is therefore measured mainly during the VD test in clinical diagnosis [3]. Therefore, human plasma/serum 25VD₃ is widely used as a biomarker [4, 5]. The standard physiological range of VD is 30–70 ng mL⁻¹ and a value below 30 ng mL⁻¹ indicates an alarming situation of VD deficiency. Hence, timely assessment of VD levels in body fluid can avoid nutritional deficiencies and also prevents irreversible damage caused to vital organs.

Currently, the analysis methods adopted for VD monitoring are liquid chromatography-mass spectrometry (LC-MS), radioimmunoassay (RIA), high-performance liquid chromatography (HPLC), and enzyme-linked immunoassays (ELISA) [6]. Although HPLC and ELISA can be routinely performed by trained technicians still these methods have some limitations. In HPLC, large quantities of expensive

✉ Pratima R. Solanki
pratimarsolanki@gmail.com; partima@mail.jnu.ac.in

¹ Special Centre for Nanoscience, Jawaharlal Nehru University, New Delhi 110067, India

organics are required that increases the cost of analysis. Also, HPLC have low sensitivity for certain compounds, and some cannot be detected as they are irreversibly adsorbed. In the case of ELISA, a format consisting of a 96-well plate is used and it requires 100–200 μL of sample for each well during testing. Such a large demand for sample volume will hinder how many targets can be quantified from the test sample and severely limit the ability to add replicates for more accurate, reliable results. The possibility of false-positive or negative results is high in ELISA due to insufficient blocking of immobilized antigen [7]. Thus, there is an urgent need to fabricate a fast and cost-effective point of care (POC) device like an immunosensor to monitor VD levels. In order to minimize delays in diagnosis, POC are useful diagnostic alternatives, which is vital since delays or ineffective procedures can result in high casualties. Chip, carbon cloth, and paper-based biosensors were established for quick detection with the improvements of POC research. It provides several incentives to users such as being affordable, flexible, sensitive, specific, user-friendly, rapid, robust, equipment-free, and deliverable [8–10]. The result can be achieved rapidly and conveniently, allowing for quick decision-making, thus minimizing the risk of human-to-human transmission. Few reports are available in the literature for the development of VD biosensors including the previous work done in our lab for VD detection [4, 11–16]. However, the biosensor developed for 25VD₃ is very limited as shown in Table 1. Ozbakir et al., reported the enzyme-modified electrode-based electrochemical detection of 25VD₃ in a range of 5–200 ng mL^{-1} [14]. The process for the synthesis of the enzyme was time-consuming and follows a long procedure to do the cloning followed by expression study, and purification of proteins. Further, Carlucci et al. detected 25VD₃ through electrochemical and surface plasmon resonance (SPR) techniques utilizing screen-printed gold (Au) electrode and sensitivity obtained as 0.020 $\mu\text{A ng}^{-1} \text{mL cm}^{-2}$ and limit of detection (LOD) as 10 ng mL^{-1} . However, the use of the Au electrode is costly, and also the SPR technique requires expertise to handle the instrument [15]. One recent report for 25VD₃ detection by Kaur et al. utilized gold-platinum bimetallic nanoparticles coated 3-(aminopropyl)triethoxysilane (APTES) for immunosensor (Ab-25(OH)D₃/Glut/Au-Pt/APTES) to detect 25VD₃ [16].

The main shortcomings of the previous reports are the lack of validation study through a conventional technique of ELISA and also the real samples were not analyzed to test the efficiency of the electrodes. Thus, there is a wide scope to fabricate VD₃ biosensors by utilizing different nanomaterials on appropriate substrates to improve the bio-sensing parameters.

Metal oxide nanostructured ceria (nCeO_2) demonstrates exciting features, and many reports are available for the detection of various analytes including glucose, DNA, cholesterol, hydrogen peroxide, cancer biomarkers, food toxins, and pesticides [17–20] for biosensor applications. Due to its unique features including electrical conductivity, nominal swelling, high mechanical strength, wide bandgap (3.4 eV), oxygen storage capacity, and ability to switch oxidation states ($\text{Ce}^{3+}/\text{Ce}^{4+}$) [19, 20]; it provides a suitable biosensing platform. Moreover, it is non-toxic, shows chemical inertness, high adsorption capability, high electron transfer kinetics, and high isoelectric point IEP (9.2) [18] which makes nCeO_2 a promising material for conjugation of desired bioactive molecules on the electrode surface.

The incorporation of nanomaterials onto a suitable substrate provides a synergetic effect to accelerate signal transduction leading to high sensitivity [21, 22]. Among other substrates, carbon-based substrate exhibits good electrocatalytic activity, fast electron transfer kinetics, non-fouling effects, biodegradable, biocompatible, and cost-effective [23, 24]. Carbon cloth (CC) is a flexible textile material and has carbon filaments of 5–10 μm in diameter. CC is different from other rigid substrates like indium tin oxide (ITO), fluorine tin oxide (FTO), and glassy carbon electrode (GCE). The application of CC as an electrode substrate provides enhanced diffusion of electrolyte and more channels to transport ion rapidly from electrolyte to electrode material [25]. In addition, CC exhibited high conductivity, chemical stability, lightweight, low-cost material, and three-dimensional structures showing its great potential in the fabrication of electrochemical biosensor. Moreover, CC possess interesting characteristics such as faster adsorption due to larger surface area, good biocompatibility, a low barrier to mass transfer. This substrate is mainly reported for supercapacitor applications. But, Mahesh et al. [26] reported an electrochemical sensor for dopamine detection. They

Table 1 Summary of the biosensors developed for VD detection until now

Electrode	Technique used	Range	LOD	Sensitivity	Ref
Ab-25OHD/SPE/FMTAD	SPR	5–50 $\mu\text{g mL}^{-1}$	1000 ng mL^{-1}	4.8 $\text{m}^\circ \text{mL } \mu\text{g}^{-1}$	[15]
	DPV	20–200 ng mL^{-1}	10 ng mL^{-1}	0.020 $\mu\text{A ng}^{-1} \text{mL cm}^{-2}$	
CYP27B1/GCE	CV	5–200 ng mL^{-1}	-	-	[14]
BSA/AB-25OHD ₃ /CAEF/RCP	Chrono amperometry	10–100 ng mL^{-1}	10 ng mL^{-1}	0.16 $\mu\text{A ng}^{-1} \text{mL cm}^{-2}$	[4]
Ab-25(OH)D ₃ /Glut/Au-Pt/APTES	DPV	0.1–10 ⁶ pg mL^{-1}	0.0049 ng mL^{-1}	-	[16]
BSA/anti-25VD ₃ /nCeO ₂ /CC	DPV	1–200 ng mL^{-1}	4.63 ng mL^{-1}	2.08 $\mu\text{A ng}^{-1} \text{mL cm}^{-2}$	Present work

studied the catalytic activity of dopamine on iron oxide nanoparticles deposited on acid-treated CC. Therefore, CC substrate can be utilized for other electrochemical biosensor fabrication.

In this work, a simple electrochemical, label-free, stand-alone, and cost-effective immunosensor has been reported for 25VD₃ detection based on nCeO₂ anchored CC. The nCeO₂ was synthesized through the bottom-up approach and anchored to the CC substrate *via* electrophoretic deposition (EPD) to obtain the nanoplatform (nCeO₂/CC). Subsequently, bioactive molecules like antibodies specific to 25VD₃ (anti-25VD₃) and bovine serum albumin (BSA) were immobilized on the nanoplatform for the development of nanobioplatform (BSA/anti-25VD₃/nCeO₂/CC) as an immunosensor. The analytical performance of the developed immunosensor was observed and the results exhibited a better sensitivity, wide detection range, and good lowest detection limit in comparison to previously reported work for 25VD₃ detection (Table 1). Moreover, the validation studies were also conducted using real samples and the results were found in good agreement with ELISA results.

Experimental techniques

Chemicals and characterization techniques

All the chemicals and reagents were of analytical grade and detailed information has been provided in the supplementary data. The detailed information of characterization techniques used for analysis is also given in the supplementary data.

Synthesis of nCeO₂ and fabrication of nanoplatform (nCeO₂/CC)

nCeO₂ was prepared by the bottom-up approach according to previous reports as mentioned in the supporting data [27, 28]. CC was utilized for the nanoplatform fabrication for which the surface of CC was pre-treated before the deposition of nCeO₂. A large piece of CC was treated with a mixture of concentrated H₂SO₄ and HNO₃ (1:3) at 80 °C for 5 h followed by washing with de-ionized water (D.I. water) and ethanol several times and dried at 60 °C for 12 h. This acid treatment promotes the activation of reactive functional groups available on CC [26]. After activation, desired dimensions (0.5 × 1.5 cm) of CC were used for the deposition of nCeO₂ using the EPD technique. For the EPD process, a suspension of nCeO₂ (2 mg mL⁻¹) was prepared in IPA through sonication for 2 h at room temperature. EPD was carried out using a two-electrode system in which CC (cathode) and a platinum wire (anode) were vertically oriented and separated by 1 cm in a container having a suspension of nCeO₂ (4 mL). A uniform and stable film (nCeO₂/CC) was fabricated using an optimized

parameter of 80 V potential for a duration of 3 min. Further, the nanoplatform was rinsed with D.I. water to remove the excess material and then left for drying at 60 °C for 12 h to improve the binding. EPD is a versatile technique and has several advantages like short deposition time, simple apparatus requirement, and suitability for mass production and hence used for the deposition of nCeO₂ onto CC. Also, EPD allows easy modifications as per the requirement of a specific application. For example, deposition can be performed on any type of substrate, viz flat, cylindrical, or any other shaped substrate with only minor changes in electrode design and positioning. Further, EPD offers easy control over the deposition thickness and morphology of deposited film by varying the deposition time and applied potential [29, 30]. The fabricated nanoplatform was observed to check the flexibility and anchoring of nCeO₂ onto CC (Supp data: Figure. S1).

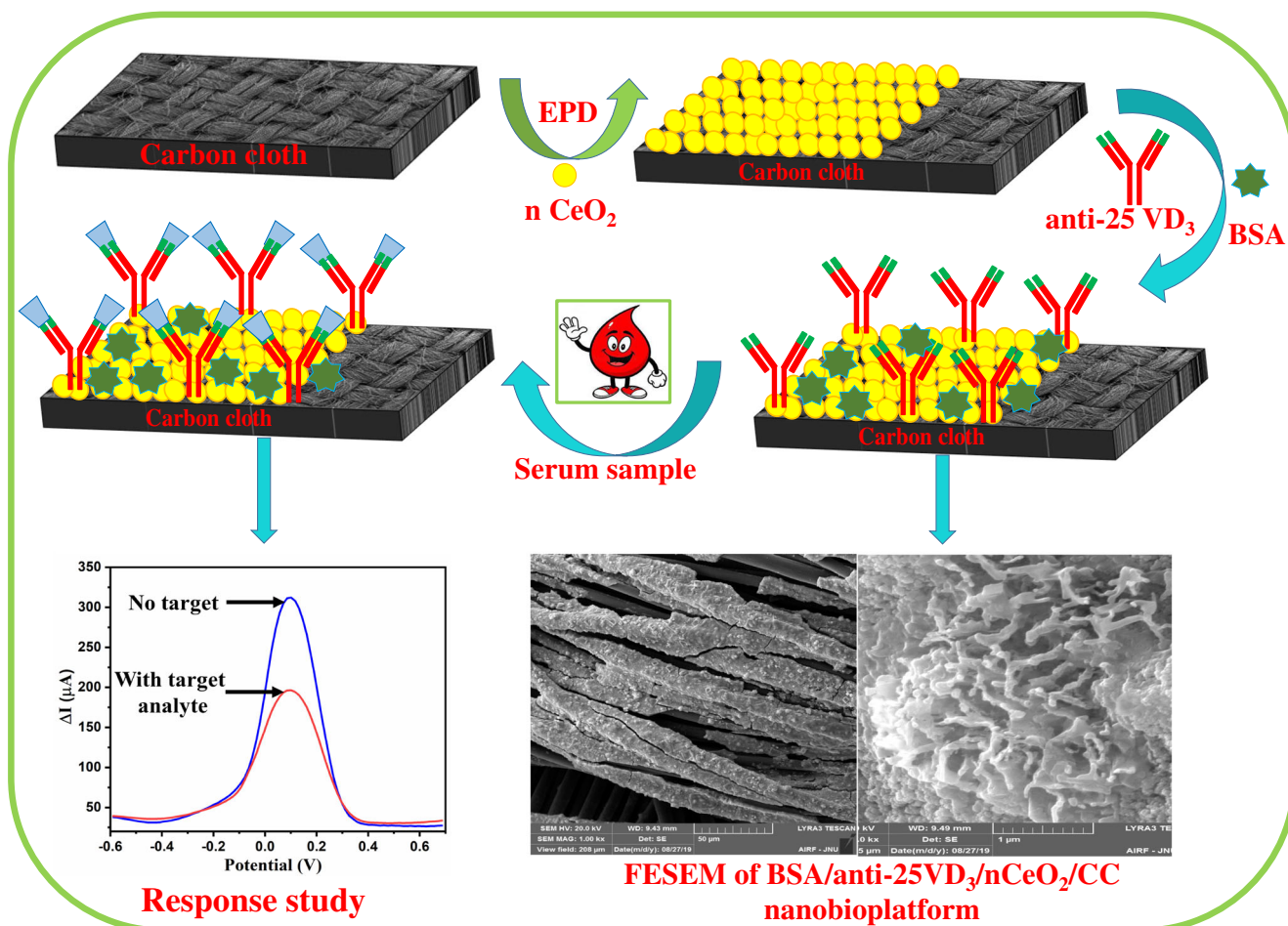
Fabrication of immunosensor through conjugation of bioactive molecules

Initially, the stock solutions of anti-25VD₃ and BSA were made in PBS saline (pH 7.0) with a concentration of 1.15 mg mL⁻¹ and 1 mg mL⁻¹, respectively. Further, a final working dilution of anti-25VD₃ (50 µg mL⁻¹) was made from the initial stock solution for further experiments. The effective conjugation of anti-25VD₃ onto the surface of nCeO₂/CC nanoplatform was done with the help of covalent binding using EDC-NHS chemistry. Solutions of anti-25VD₃, NHS (0.1 M), and EDC (0.4 M) were prepared by mixing them in a ratio of 2:1:1 (v/v) and kept for about 30 min at 4 °C resulting in activation of anti-25VD₃ carboxyl (COO⁻) groups. Thereafter, 20 µL solution of activated anti-25VD₃ was drop cast onto nCeO₂/CC nanoplatform and kept in a humid chamber for 6 h so that activated anti-25VD₃ binds effectively with nCeO₂. This fabricated nanobioplatform anti-25VD₃/nCeO₂/CC was washed with PBS for the removal of excess anti-25VD₃ from the surface. The blocking of non-binding sites was done by introducing 10 µL of BSA onto nanobioplatform (anti-25VD₃/nCeO₂/CC) and incubated for 4 h. The obtained BSA/anti-25VD₃/nCeO₂/CC nanobioplatform was washed with PBS and stored at 4 °C to maintain the activity of the immobilized bioactive molecules (BSA and anti-25VD₃). The stepwise fabrication process of the immunosensor is illustrated in Scheme 1.

Results and discussions

Characterization of nCeO₂

To identify the crystallographic structure of nCeO₂, XRD analysis was done and the XRD patterns (Fig. 1) showed eight well-resolved and intense peaks in the range of 2θ = 10–80°. The diffraction peaks appeared at an angle (2θ) were 28.56,



Scheme 1 Fabrication process of immunosensor BSA/anti-25VD₃/nCeO₂/CC

33.01, 47.50, 56.20, 59.10, 69.35, 76.69, and 78.99 which correspond to the crystal planes ascribed as (111), (200), (220), (311), (222) (400), (311), and (420), respectively [27, 31]. The XRD pattern demonstrated that all characteristic peaks are remarkably close to the face-centered-cubic (fcc) fluorite structure of CeO₂ crystal (JCPDS: 34-0394). The fluorite structure consists of an arrangement where each cerium atom is surrounded by 8 oxygen atoms in an fcc arrangement and each oxygen atom has a cerium atom in a tetrahedron arrangement around it. No other peak was detected indicating the good crystallinity and preparation of nCeO₂ in the pure phase.

The average crystallite size corresponds to the highest intensity peak (111) which was calculated using the Debye Scherer equation and found to be 10.35 nm. The formula used for the calculation is as below:

$$D = K\lambda / \beta \cos\theta \quad (1)$$

where K is the Scherer constant having a value in the range of 0.9 to 1, β denotes the full width at half maximum of various diffraction peaks, θ denotes Bragg's diffraction angle, and λ shows the wavelength of target Cu-K α .

The morphology and size of synthesized nCeO₂ were observed using TEM studies. Figure 1 (b–d) shows TEM, HR-TEM, and selected area electron diffraction (SEAD) patterns, respectively. It is apparent from image (b) that almost all nanoparticles were spherical in shape, well dispersed, and uniform in size. Image (c) shows the well-resolved HR-TEM image that is comprised of organized lattice planes of nCeO₂ with a cubic phase. The continuous and clearly visible lattice fringes are indicative of the crystallinity of nCeO₂. Further, the interfringe distances (d) of 0.33 nm calculated using ImageJ software can be indexed to the (111) plane of cubic nCeO₂ and strongly supported the XRD data. The inset of image (c) shows the particle size distribution graph which revealed the average size of nCeO₂ to be 14.38 ± 1.5 nm. The SEAD pattern (image d) showed very bright spots of the rings which revealed the highly crystalline nature of nCeO₂. The bright spots obtained on these rings were well indexed to (222), (220), (220), and (111) planes of cubic nCeO₂ (JCPDS card 34-0394).

FTIR, Raman, and UV-visible spectroscopy (Fig. 2) techniques were employed to confirm the synthesis of nCeO₂. FT-IR spectrum analysis of nCeO₂ (image a) shows some

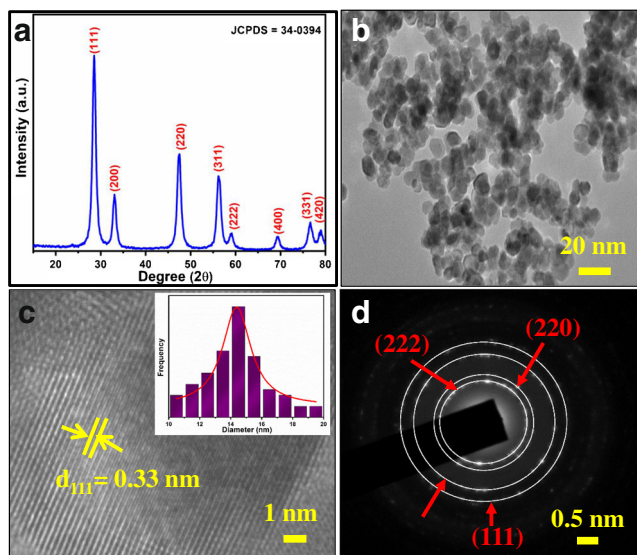


Fig. 1 (a) XRD spectrum of nCeO₂, (b) TEM image, (c) HR-TEM image (inset shows size distribution of nCeO₂), and (d) SEAD pattern for nCeO₂, respectively

absorption bands in the region of 400 to 4000 cm⁻¹. The band appeared at 660 cm⁻¹ corresponds to Ce-O stretching vibration. Another stretching band observed at 1320 cm⁻¹ revealed carbonate-like species (O-C-O). The next band at 1635 cm⁻¹ represents the “scissor” bending mode of molecular H₂O (H-O-H). Finally, a broad absorption band at 3410 cm⁻¹ corresponds to -OH stretching vibration mode of (H-bonded) water molecules present due to physically absorbed H₂O or surface -OH groups, respectively [32–34].

Figure 2 (b) shows the Raman spectrum of nCeO₂ which exhibits one strong peak at 465 cm⁻¹ and three other peaks of low intensity at 270, 605, and 1051 cm⁻¹. The strong peak at 465 cm⁻¹ belongs to the first-order Raman line and represents the characteristic peak of the cubic form of nCeO₂ [33]. This peak may be attributed to triply degenerated Raman active optical phonon mode (F_{2g}). The shoulder peak at 270 cm⁻¹ is attributed to transverse optical (TO) doubly degenerate mode. Further, another two peaks at 605 and 1051 cm⁻¹ belong to the second-order Raman line and were assigned to the longitudinal optical (LO) mode. Due to the

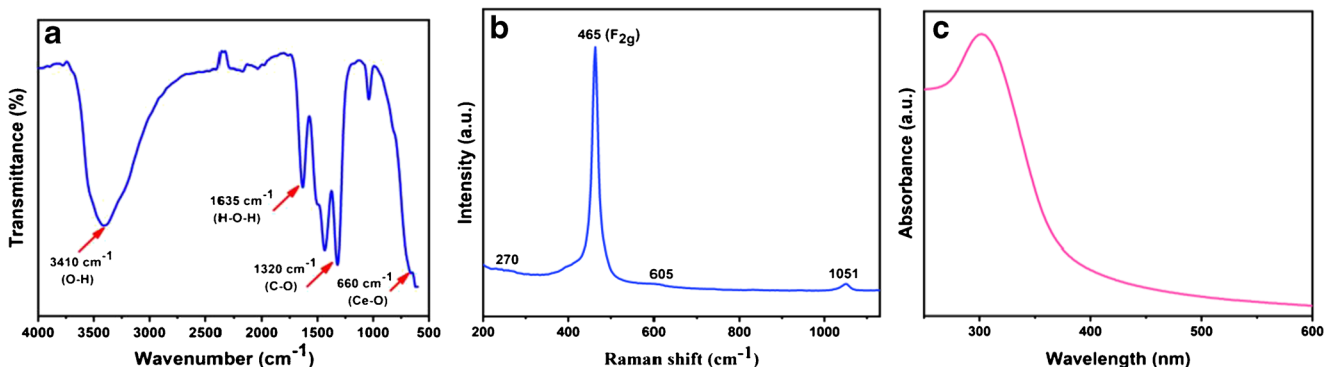


Fig. 2 (a) FTIR spectrum, (b) Raman spectrum, and (c) UV-visible spectrum of nCeO₂

presence of oxygen vacancies and the intrinsic defects in the nCeO₂, a peak at 605 cm⁻¹ was observed [35]. Also, the Raman analysis confirms the presence of a cubic fluorite structure with oxygen vacancies in the synthesized nCeO₂.

Figure 2 (c) shows the UV/Vis absorption spectrum of synthesized nCeO₂ (dispersed in D.I. water), recorded in the range of 250–600 nm. The spectrum showed a strong absorption peak at 310 nm which is due to charge-transfer transitions from O atom through 2p orbital to Ce atom in 4f orbital [33, 36].

All these spectroscopic characterizations clearly supported the successful synthesis of nCeO₂ without any impurity.

Characterization of nCeO₂/CC nanoplatform and BSA/anti-25VD₃/nCeO₂/CC immunoelectrode

Figure 3 (a–c) shows the morphology of nCeO₂/CC nanoplatform and images (d–f) represent the conjugation of bioactive molecules (anti-25VD₃ and BSA) on the surface of nCeO₂/CC nanoplatform, using the FE-SEM technique. Image (a) shows the FE-SEM image of nCeO₂/CC nanoplatform where CC appears to be fibrous and deposition of nCeO₂ onto this fibrous CC is also visible. However, image (b) shows the rough surface due to the uniform deposition of nCeO₂, which provides a suitable platform for the immobilization of bioactive molecules. Figure 3 (c) shows the magnified view of nCeO₂/CC nanoplatform which suggests a globular morphology of uniformly deposited nCeO₂ (spherical shaped) that are embedded onto the fibrous structure of CC. Therefore, good contact was established between nCeO₂ and CC fibers.

Figure 3 (d, e, and f) shows the morphology of biomolecules conjugated nCeO₂/CC nanoplatform. Image (d) reveals the increment in the roughness and appearance of some island like entities at the surface. This large increment in roughness and alteration in morphology is due to the conjugation of bioactive molecules onto the surface of the nCeO₂/CC nanoplatform. Image (f) also shows the appearance of some Y-shaped structures bound to nCeO₂ due to the presence of anti-25VD₃ attachment. All these morphological changes revealed the successful conjugation of bioactive molecules and the fabrication of immunosensor (BSA/anti-VD₃/nCeO₂/CC).

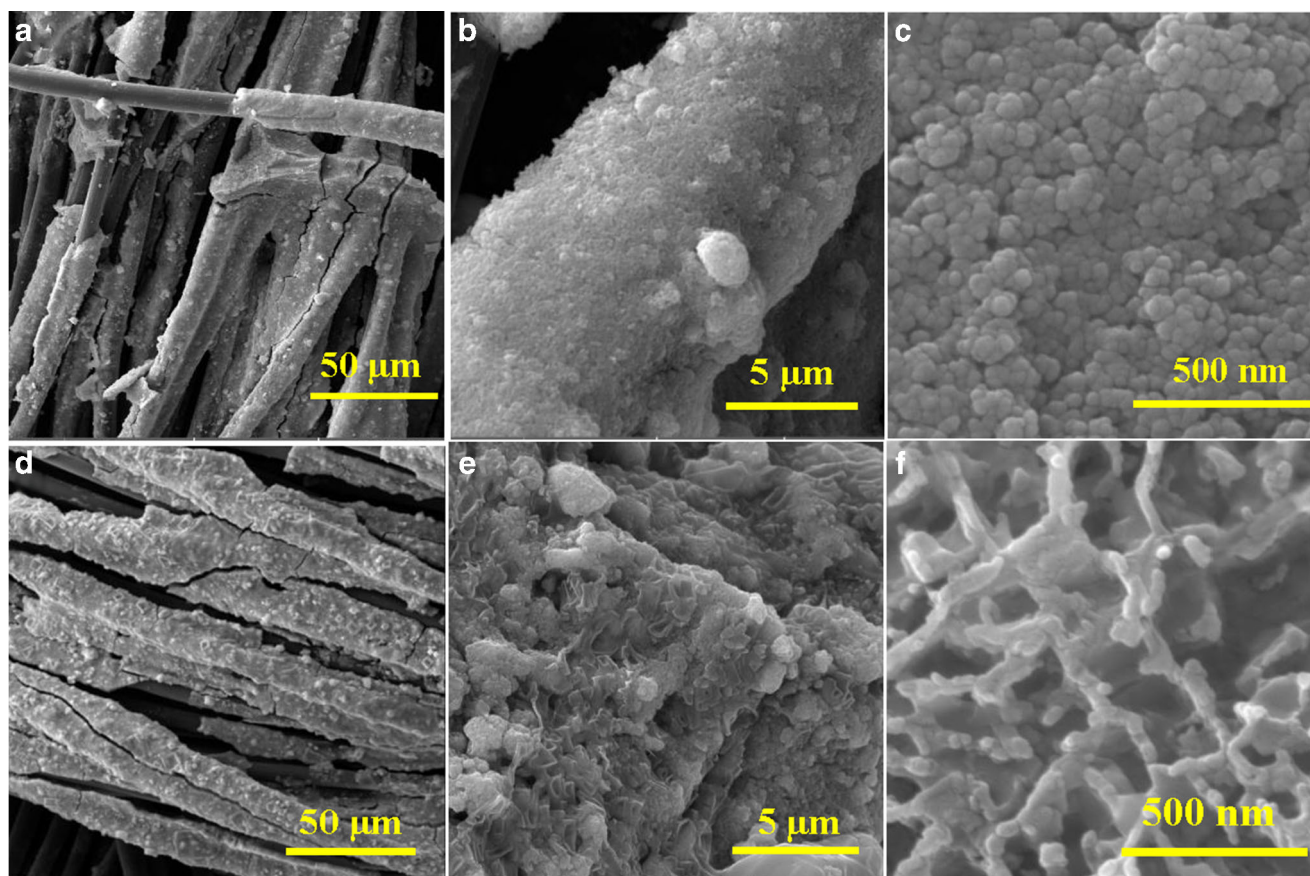


Fig. 3 (a, b, and c) FE-SEM images of nCeO₂/CC nanoplatform, and (d, e, and f) BSA/anti-VD₃/nCeO₂/CC immunosensor at different scales, respectively

Electrochemical studies

The electrochemical techniques such as cyclic voltammetry (CV) and differential pulse voltammetry (DPV) measurements were carried out for characterization as well as for label-free detection of 25VD₃. All measurements were done in PBS (0.1 M, pH 7.0, 0.9% NaCl) containing 5 mM of [Fe(CN)₆]^{3-/4-} as a redox probe using a conventional three-electrode system. The three-electrode system has the BSA/anti-25VD₃/nCeO₂/CC immunoelectrode (0.25 cm²) as a working electrode, an Ag/AgCl reference electrode, and platinum wire (0.25 mm) as the counter electrode. CV was carried out at a scan rate of 50 mV s⁻¹ in the potential range of -0.6 V to 0.8 V, while DPV was recorded in a potential range of -0.6 V to 0.7 V with a pulse width of 50 ms and pulse height of 25 mV.

pH study and electrochemical characterization studies

The influence of different pH of PBS ranging from 6.0 to 8.0 was evaluated to analyze the behavior of antibodies [37] present on the immunosensor (BSA/anti-25VD₃/nCeO₂/CC) and the highest peak current was found at pH 7.0 (Figure S2).

Figure 4 (a) shows the CV of (i) bare ITO, (ii) CC, (iii) nCeO₂/CC, (iv) anti-25VD₃/nCeO₂/CC, and (v) BSA/anti-

25VD₃/nCeO₂/CC immunosensor in PBS (pH 7.0) containing [Fe(CN)₆]^{3-/4-} as a redox probe. CC exhibited oxidation and reduction in peak current much higher (1118.6 μA) than that of ITO (367 μA) which is a typical characteristic of CC. The higher current value obtained is due to the good electrical conductivity, larger specific surface area and a higher carbonization degree of CC. After the inclusion of nCeO₂, the oxidation peak current is enhanced to 1855.6 μA (curve iii; nCeO₂/CC nanoplatforms). This confirms the deposition of nCeO₂ onto CC and increases the overall electroactive surface of the nanoplatforms, resulting in acceleration of electron transport between the redox probe and the platform surface [38]. The magnitude of the current was decreased to 1480.7 μA (curve iv) after the conjugation of anti-25VD₃ and to 1342.6 μA (curve v) after BSA immobilization. This decrease could be attributed to the insulating effect of bioactive molecules (anti-25VD₃ and BSA) that obstructed the diffusion of the electrons generated from the redox probe to the platform surface [39], which confirmed the sequential modification. These CV results were found in good agreement with DPV results (Fig. 4 (b)). Moreover, electrochemical impedance spectroscopy (EIS) study has been performed which further support sequential modification of electrodes (Fig. S3).

Besides this, the evaluation of the scan rate effect from 10 to 100 mV s^{-1} has been done to explain the electrochemical activity of fabricated nCeO_2/CC nanoplatform and BSA/anti-25VD₃/ nCeO_2/CC immunosensor (Figure S4). The variation of anodic and cathodic peak currents ($I_{\text{pa}}/I_{\text{pc}}$) as a function of the square root of the scan rates (\sqrt{v}) showed a straight line and the value of $I_{\text{pa}}/I_{\text{pc}}$ was found as ~ 1 for BSA/anti-25VD₃/ nCeO_2/CC immunoelectrode revealing the transfer to be quasi-reversible kinetics. Also, for both platforms, the peak current I_{pa} (anodic) and I_{pc} (cathodic) were increased linearly with \sqrt{v} , indicating a diffusion-controlled process between the immunosensor surface and the redox probe.

Analytical performance of the immunosensor

The response of the fabricated immunosensor (BSA/anti-25VD₃/ nCeO_2/CC) was studied as a function of 25VD₃. The optimization of incubation time for the interaction of 25VD₃ (1 ng mL^{-1}) with the immunosensor platform was conducted at an interval of 3 min (Fig. 5 (a)) up to 15 min. The peak current was decreased from 0 to 9 min and then became almost constant from 10 to 15 min. Therefore, 15 min was set as an optimized incubation time for the response studies.

The response of the developed immunosensor towards detection of 25VD₃ from 1 to 200 ng mL^{-1} was measured through the DPV technique. The decreasing trend in peak current was found after the addition of each 25VD₃ concentration (Fig. 5 (b)) and became constant at 180 ng mL^{-1} . The decreasing trend in the peak current was attributed to the interaction of 25VD₃ with anti-25VD₃ that led to the formation of an electrically insulating complex. This complex obstructed the transfer of electrons between the redox probe and immunosensor. A 200 ng mL^{-1} of 25VD₃ concentration was found enough for saturation of available anti-25VD₃ present on the nanobioplatform surface. Here, 1 ng mL^{-1} was the

lowest concentration of 25VD₃ that could be detected with the present immunosensor.

The mechanism behind the decreasing trend in the peak current was attributed to the charge transfer factor and shift in the Fermi level between nCeO_2 and bioactive molecules. The size of 25VD₃ is bulky in comparison to nCeO_2 (nm), therefore preventing the flow of electrons to immunosensor from the redox probe. The chemical bond formation between the bioactive molecules (anti-25VD₃, BSA, and 25VD₃) at the semiconductor surface (nCeO_2) is analyzed that showed the presence of two factors contributing to adsorption energy: one is bond creation and the second is charge transfer. The charge transfer factor decides the direction of the Fermi level shift in the bandgap region either from semiconductor to bioreceptors or vice versa. Electron transfer from the 25VD₃ molecule will take place to the conduction band of the working electrode followed by the transition to its valence band leading to electron-hole (e-h) pair recombination. As a result, the hole concentration in the valence band will be reduced; consequently, the extrinsic Fermi level will be shifted away from the valence band, leading to downward band bending and a decrease in the current trend [40].

Figure 5 (c) shows the calibration curve between the change in peak current obtained through the DPV study and the 25VD₃ concentrations. The calibration curve clearly revealed a linear and inverse relationship between current values and 25VD₃ concentrations. The experiments were repeated thrice and the error bar shows the standard deviation. Sensitivity was estimated from the formula: calibration curve slope/surface area of immunosensor (0.25 cm^2) and found to be 2.08 $\mu\text{A ng}^{-1} \text{mL cm}^{-2}$ with R^2 of 0.989. The immunosensor lower detection limit and the linear range were observed as 4.63 ng mL^{-1} and 1–160 ng mL^{-1} , respectively. These obtained biosensing parameters of are much better than the previously reported biosensors (Table 1). All the

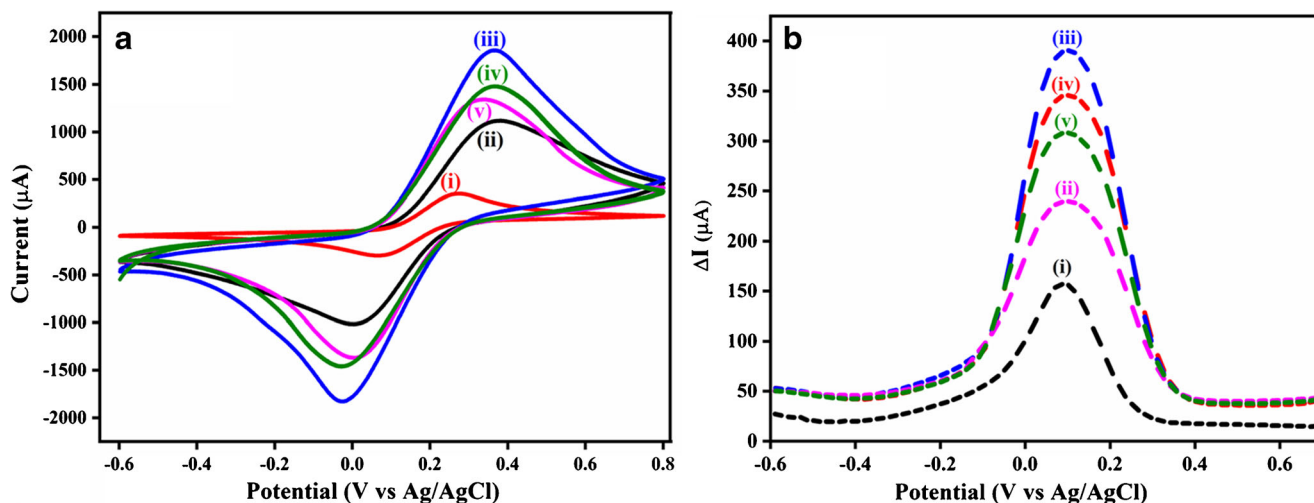


Fig. 4 (a) CV and (b) DPV studies of (i) ITO, (ii) CC, (iii) nCeO_2/CC , (iv) anti-25VD₃/ nCeO_2/CC , and (v) BSA/anti-25VD₃/ nCeO_2/CC immunosensor, respectively

measurements were performed three times to check the repeatability and reproducibility of the developed immunosensor.

The linear plot between peak current and 25VD₃ concentration provided the equation:

$$I_p = 0.52 \text{ conc. (ng mL}^{-1}\text{)} + 292.18 \mu\text{A}, R^2 = 0.989 \quad (2)$$

Specificity, reproducibility, and stability

Specificity is an important and vital parameter for the majority of the biosensor as the nonspecific bindings can hinder and mislead the results of 25VD₃ detection. Thus, the specificity of the fabricated immunosensor was evaluated by introducing some interfering species that are present in serum samples such as glucose (GLU), ascorbic acid (AA), urea, uric acid (UA), and oxalic acid (OA) and keeping a 25VD₃ concentration of 100 ng mL⁻¹ onto BSA/anti-25VD₃/nCeO₂/CC immunosensor. The evaluation has been shown in terms of a

bar graph (Fig. 6 (a)). Results revealed an excellent specificity of immunosensor towards detection of 25VD₃. Biosensors are specific in nature rather than selective as the development of a biosensor is based on the utilization of bioactive molecules (antibody, enzyme, tissue, etc.) which are specific to their respective analyte. The present immunosensor utilized antibodies (anti-25VD₃) specific to the target analyte (25VD₃) and hence detect 25VD₃ significantly and did not respond to other interfering species. However, the fabricated platform nCeO₂/CC can be applied for the detection of various other diagnostic biomarkers (vitamins, cancer, food toxins, antibiotics, and pesticides, etc.) by simply changing the analyte-specific bioactive molecules.

Six different nanobioplatfroms (BSA/anti-25VD₃/nCeO₂/CC) were prepared under similar conditions and used individually for reproducibility studies (Fig. 6 (b)). The peak value of all independent electrodes remained nearly the same and the value of RSD was calculated to be 4.62%, suggesting high precision and acceptable range. This showed that the

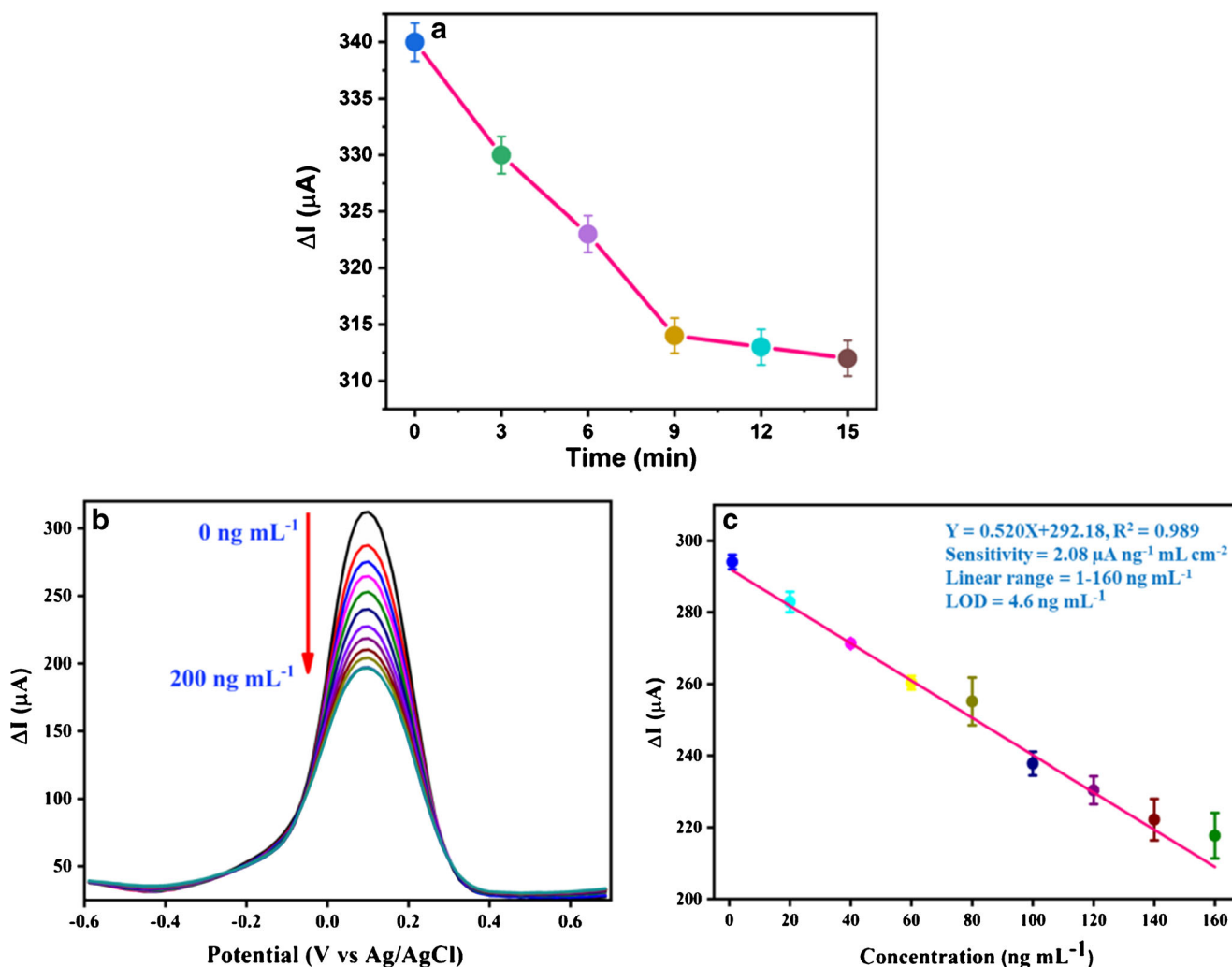


Fig. 5 (a) Incubation time study, (b) analytic performance of BSA/anti-25VD₃/nCeO₂/CC immunosensor in term of DPV as a function of 25VD₃ concentration (1–200 ng mL⁻¹), and (c) calibration plot of peak current and 25VD₃ concentrations

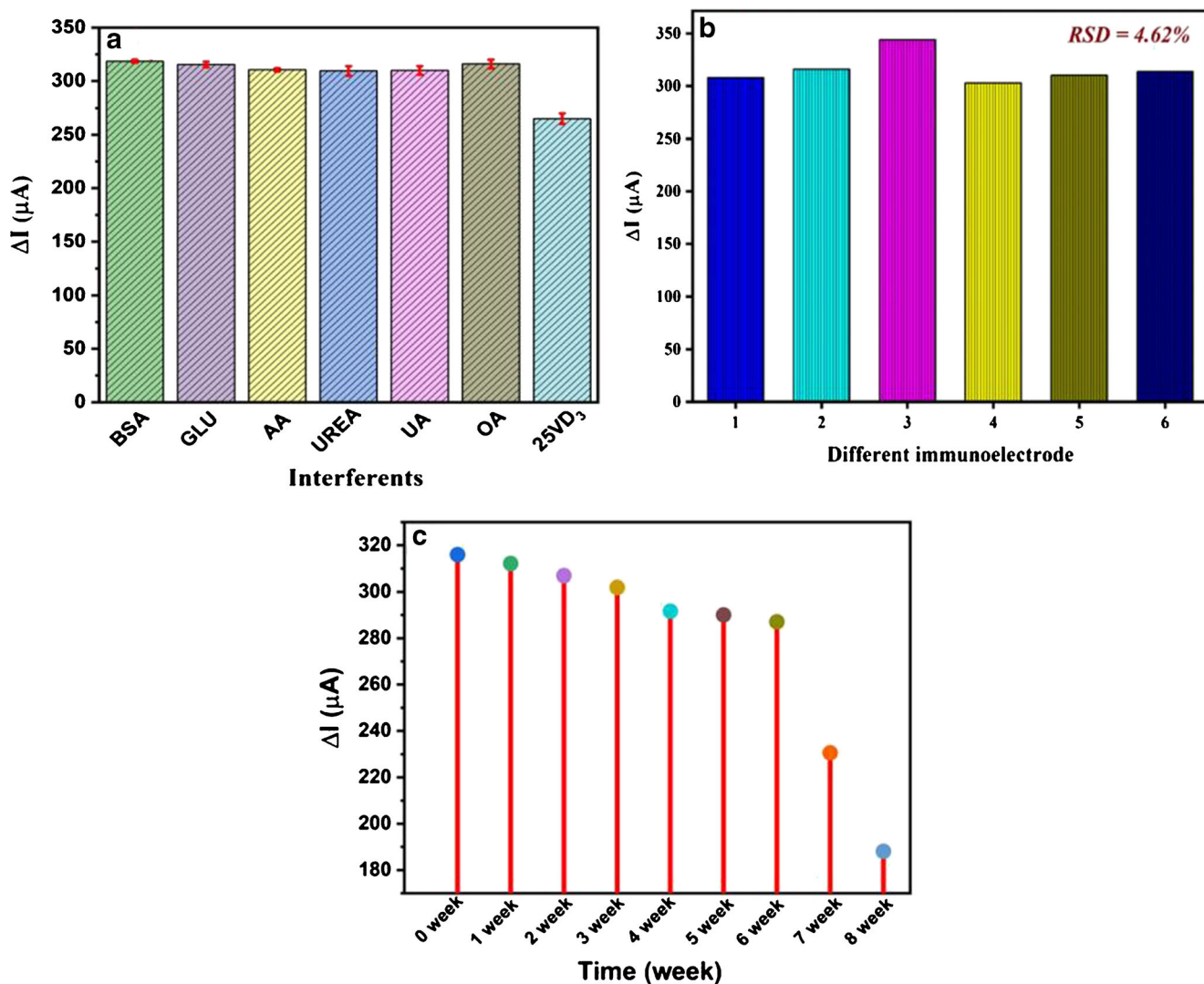


Fig. 6 (a) Specificity, (b) reproducibility, and (c) stability of fabricated BSA/anti-25VD₃/nCeO₂/CC immunosensor

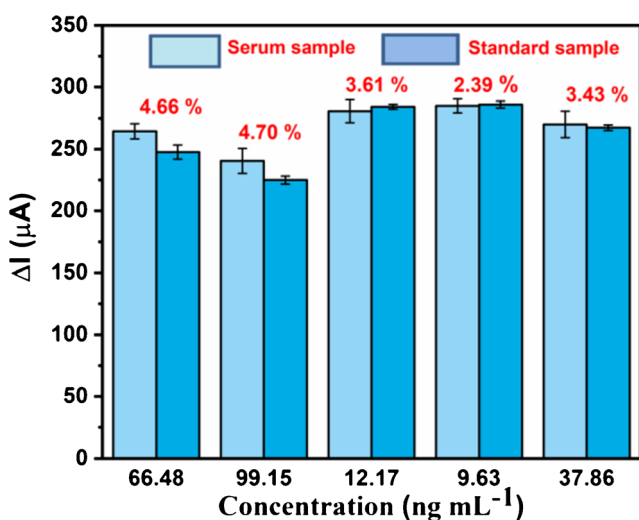


Fig. 7 Serum sample analysis onto fabricated BSA/anti-25VD₃/nCeO₂/CC immunosensor

fabricated immunosensor represented good reproducibility apart from specificity.

Moreover, the stability of fabricated immunosensor is a key factor that must be observed over a period of time and it was determined by observing the value of peak current after a regular interval of 1 week for 8 weeks. As shown in Fig. 6 (c), the value of peak current showed a certain degree of decrease which was not significant for up to 6 weeks. The obtained results revealed excellent stability of immunosensor for about 45 days. After 6 weeks, a notable decrease in peak current was observed which was almost 30% of the initial peak current value. The decrease became almost 50% after 8 weeks of the time.

Generally, the stability of a biosensor is influenced by degradation of the bioactive molecules over a period of time [41, 42]. Hence, in the present immunosensor, the reason of performance deterioration in the stability is due to the activity loss of the antibodies (anti-25VD₃).

ELISA and real sample analysis

The serum samples were obtained from U Healthcare & Diagnostic Laboratory, New Delhi (India). The quantification of serum samples was done with ELISA using a kit having an antigen (25VD₃) precoated 96-well plate in triplicate. ELISA was performed according to manual instructions and absorbance was recorded using an ELISA plate reader (450 nm) to get the quantified concentration of serum samples. The obtained concentrations of 25VD₃ in serum samples were 66.48, 99.15, 12.17, 9.63, and 37.68 ng mL⁻¹ as shown in the second column of Table S3. After quantification, serum samples were incubated for 15 min and electrochemical analysis (DPV response) was observed onto the fabricated immunosensor to check its performance towards serum samples. It was found that a reasonable correlation existed between the magnitude of the DPV current response of the fabricated immunosensor incubated with the serum samples (25VD₃ determined by ELISA) and with the standard 25VD₃ concentrations (Fig. 7). The observed results exhibited % RSD values less than 10% indicating high accuracy of fabricated immunosensor. A tabular representation for the serum sample analysis is also summarized in Table S3.

Conclusion

Here, a novel electrochemical immunosensor based on CC for detection of 25VD₃ was proposed. nCeO₂ was synthesized through a simple bottom-up approach and further utilized for immunosensor development. EPD was applied for anchoring nCeO₂ onto CC to get a highly conductive nCeO₂/CC nanoplatform. CC confers higher conductivity and provides a large surface area than other substrates (ITO, GCE, etc.) and the inclusion of nCeO₂ onto CC facilitates faster electron transfer. The developed immunosensor showed excellent biosensing parameters along with high specificity, reproducibility, and stability. The proposed immunosensor was then applied to detect 25VD₃ levels in human serum samples. The immunosensor showed promising results and faster detection (15 min) compared to traditional methods of ELISA with acceptable relative error. This study proves the combination of CC and nCeO₂ as a promising platform for biosensor development because of their remarkable properties. It is to be noted that CC-based low-cost, disposable, and highly electroactive-based nanobioplatform added advantages towards the production of wearable sensors, developing lab-on-biochip and POC diagnosis platforms. However, in the present work, drop cast was not successful to fabricate the nanoplatform as CC is permeable. Hence, to overcome this, EPD was applied for anchoring nCeO₂ onto CC to get a tightly bound and highly conductive nCeO₂/CC nanoplatform that can adhere the bioactive molecules well

onto its surface to develop immunosensor. Further, we believe that the developed platform can be applied for the detection of different diagnostic biomarkers just by replacing the bioreceptors specific to target analyte.

Supplementary Information The online version contains supplementary material available at <https://doi.org/10.1007/s00604-021-04751-y>.

Acknowledgments The authors thank AIRF, JNU, for the characterization facilities of TEM, and FESEM. We sincerely thank to Kashyap Dave at SCNS, JNU, for his guidance and constant help towards CC.

Funding This work received financial supports from the Government of India through Indo-Russia (DBT/IC-2/Indo-Russia/2017-19/02), DST Purse. Deepika Chauhan received funding from UGC through the UGC-SRF scheme.

Compliance with ethical standards

Conflict of interest The authors declare no competing interests.

References

- Adela R, Borkar RM, Bhandi MM, Vishwakarma G, Reddy PNC, Srinivas R, Banerjee SK (2016) Lower vitamin D metabolites levels were associated with increased coronary artery diseases in type 2 diabetes patients in India. *Scientific reports* 6(1):1–13
- Dalgard, Christine, Maria ska alum Petersen, Pal Weihe, and Philippe Grandjean. "Vitamin D status in relation to glucose metabolism and type 2 diabetes in septuagenarians." *Diabetes Care* 34, no. 6 (2011): 1284–1288
- Rezayi M, Ghayour-Mobarhan M, Sany SBT, Fani M, Avan A, Pasdar Z, Ferns GA, Abouzari-Lotf E, Amiri IS (2018) A comparison of analytical methods for measuring concentrations of 25-hydroxy vitamin D in biological samples. *Anal Methods* 10(47): 5599–5612
- Chauhan D, Solanki PR (2019) Hydrophilic and insoluble electrospun cellulose acetate fiber-based biosensing platform for 25-hydroxy vitamin-D₃ detection. *ACS Applied Polymer Materials* 1(7):1613–1623
- Pilz S, Zittermann A, Trummer C, Theiler-Schwetz V, Lerchbaum E, Keppel MH, Grübler MR, März W, Pandis M (2019) Vitamin D testing and treatment: a narrative review of current evidence. *Endocrine connections* 8(2):R27–R43
- Yin S, Yang Y, Wu L, Li Y, Sun C (2019) Recent advances in sample preparation and analysis methods for vitamin D and its analogues in different matrices. *TrAC Trends Anal Chem* 110: 204–220
- Sakamoto S, Putalun W, Vimolmangkang S, Phoolcharoen W, Shoyama Y, Tanaka H, Morimoto S (2018) Enzyme-linked immunosorbent assay for the quantitative/qualitative analysis of plant secondary metabolites. *J Nat Med* 72(1):32–42
- Kaushik AK, Dhau JS, Gohel H, Mishra YK, Kateb B, Kim N-Y, Goswami DY (2020) Electrochemical SARS-CoV-2 sensing at point-of-care and artificial intelligence for intelligent COVID-19 management. *ACS Applied Bio Materials* 3(11):7306–7325
- Kaushik, Ajeet, and Mubarak A. Mujawar. "Point of care sensing devices: better care for everyone." (2018): 4303
- Kaushik A (2019) Biomedical nanotechnology related grand challenges and perspectives. *Front Nanotechnol* 1:1

11. Chauhan D, Gupta PK, Solanki PR (2018) Electrochemical immunosensor based on magnetite nanoparticles incorporated electrospun polyacrylonitrile nanofibers for vitamin-D₃ detection. *Mater Sci Eng C* 93:145–156
12. Chauhan D, Kumar R, Panda AK, Solanki PR (2019) An efficient electrochemical biosensor for vitamin-D₃ detection based on aspartic acid functionalized gadolinium oxide nanorods. *Journal of Materials Research and Technology* 8(6):5490–5503
13. Sarkar T, Bohidar HB, Solanki PR (2018) Carbon dots-modified chitosan based electrochemical biosensing platform for detection of vitamin D. *Int J Biol Macromol* 109:687–697
14. Ozbakir HF, Sambade D, Majumdar S, Linday L, Banta S, West AC (2015) Detection of 25-hydroxyvitamin D₃ with an enzyme modified electrode. *J. Biosens Bioelectron* 7:193
15. Carlucci, Luciano, Gabriele Favero, Cristina Tortolini, Massimo Di Fusco, Elisabetta Romagnoli, Salvatore Minisola, and Franco Mazzei. "Several approaches for vitamin D determination by surface plasmon resonance and electrochemical affinity biosensors." *Biosens Bioelectron* 40, no. 1 (2013): 350–355
16. Kaur A, Kapoor S, Bharti A, Rana S (2020) Ganga Ram Chaudhary, and Nirmal Prabhakar. Gold-platinum bimetallic nanoparticles coated 3-(aminopropyl) triethoxysilane (APTES) based electrochemical immunosensor for vitamin D estimation. *Journal of Electroanalytical Chemistry* 873:114400
17. Ansari AA, Solanki PR, Malhotra BD (2009) Hydrogen peroxide sensor based on horseradish peroxidase immobilized nanostructured cerium oxide film. *Journal of Biotechnology* 142(2):179–184
18. Pachauri N, Dave K, Dinda A, Solanki PR (2018) Cubic CeO₂ implanted reduced graphene oxide-based highly sensitive biosensor for non-invasive oral cancer biomarker detection. *J Mater Chem B* 6(19):3000–3012
19. Charbgoon F, Ramezani M, Darroudi M (2017) Bio-sensing applications of cerium oxide nanoparticles: advantages and disadvantages. *Biosens Bioelectron* 96:33–43
20. Nesakumar N, Sethuraman S, Krishnan UM, Rayappan JBB (2013) Fabrication of lactate biosensor based on lactate dehydrogenase immobilized on cerium oxide nanoparticles. *J Colloid Interface Sci* 410:158–164
21. Jianrong C, Yuqing M, He N, Wu X, Sijiao L (2004) Nanotechnology and biosensors. *Biotechnol Adv* 22(7):505–518
22. Zhu C, Yang G, He L, Dan D, Lin Y (2015) Electrochemical sensors and biosensors based on nanomaterials and nanostructures. *Anal Chem* 87(1):230–249
23. Cincy J, Milja TE, Prathish KP (2017) Fabrication of a flexible carbon cloth based solid contact iodide selective electrode. *Anal Methods* 9(20):2947–2956
24. Ye D, Yu Y, Tang J, Lin L, Yue W (2016) Electrochemical activation of carbon cloth in aqueous inorganic salt solution for superior capacitive performance. *Nanoscale* 8(19):10406–10414
25. Chen T, Li X, Qiu C, Zhu W, Ma H, Chen S, Meng O (2014) Electrochemical sensing of glucose by carbon cloth-supported Co₃O₄/PbO₂ core-shell nanorod arrays. *Biosens Bioelectron* 53: 200–206
26. Mahesh KPO, Shown I, Chen L-C, Chen K-H, Tai Y (2018) Flexible sensor for dopamine detection fabricated by the direct growth of α -Fe₂O₃ nanoparticles on carbon cloth. *Appl Surf Sci* 427:387–395
27. Chen H-I, Chang H-Y (2004) Homogeneous precipitation of cerium dioxide nanoparticles in alcohol/water mixed solvents. *Colloids Surf A Physicochem Eng Asp* 242(1–3):61–69
28. Chen HI, Chang HY (2005) Synthesis of nanocrystalline cerium oxide particles by the precipitation method. *Ceram Int* 31:795–802
29. Besra L, Liu M (2007) A review on fundamentals and applications of electrophoretic deposition (EPD). *Prog Mater Sci* 52(1):1–61
30. Liu Y, Ren L, Zhang Z, Qi X, Li H, Zhong J (2016) 3D binder-free MoSe₂ nanosheets/carbon cloth electrodes for efficient and stable hydrogen evolution prepared by simple electrophoresis deposition strategy. *Sci Rep* 6(1):1–9
31. Gao W, Zhang Z, Li J, Ma Y, Yongquan Q (2015) Surface engineering on CeO₂ nanorods by chemical redox etching and their enhanced catalytic activity for CO oxidation. *Nanoscale* 7(27): 11686–11691
32. Krishnamoorthy, Karthikeyan, Murugan Veerapandian, Ling-He Zhang, Kyusik Yun, and Sang Jae Kim. "Surface chemistry of cerium oxide nanocubes: toxicity against pathogenic bacteria and their mechanistic study." *J Ind Eng Chem* 20, no. 5 (2014): 3513–3517
33. Liu YH, Zuo JC, Ren XF, Yong L (2014) Synthesis and character of cerium oxide (CeO₂) nanoparticles by the precipitation method. *Metalurgija* 53(4):463–465
34. Zamiri R, Ahangar HA, Kaushal A, Zakaria A, Zamiri G, Tobaldi D, Ferreira JMF (2015) Dielectrical properties of CeO₂ nanoparticles at different temperatures. *PLoS One* 10(4):e0122989
35. Dhiman TK, Lakshmi GBVS, Roychoudhury A, Jha SK, Solanki PR (2019) Ceria-Nanoparticles-Based Microfluidic Nanobiochip Electrochemical Sensor for the Detection of Ochratoxin-A. *ChemistrySelect* 4(17):4867–4873
36. Jayakumar G, Albert Irudayaraj A, Dhayal Raj A (2017) Particle size effect on the properties of cerium oxide (CeO₂) nanoparticles synthesized by hydrothermal method. *Mechanics, Materials Science & Engineering Journal* 9(1)
37. Umar A, Rahman MM, Al-Hajry A, Hahn YB (2009) Highly-sensitive cholesterol biosensor based on well-crystallized flower-shaped ZnO nanostructures. *Talanta* 78(1):284–289
38. Solanki PR, Dhand C, Kaushik A, Ansari AA, Sood KN, Malhotra BD (2009) Nanostructured cerium oxide film for triglyceride sensor. *Sensors and Actuators B: Chemical* 141(2):551–556
39. Garg M, Chatterjee M, Sharma AL, Singh S (2020) Label-free approach for electrochemical ferritin sensing using biosurfactant stabilized tungsten disulfide quantum dots. *Biosens Bioelectron* 151:111979
40. Gulati P, Kaur P, Rajam MV, Srivastava T, Mishra P, Islam SS (2019) Vertically aligned multi-walled carbon nanotubes based flexible immunosensor for extreme low level detection of multidrug resistant leukemia cells. *Sensors and Actuators B: Chemical* 301: 127047
41. Zhang Y, Wei Q (2016) The role of nanomaterials in electroanalytical biosensors: a mini review. *J Electroanal Chem* 781:401–409
42. Bhakta SA, Evans E, Benavidez TE, Garcia CD (2015) Protein adsorption onto nanomaterials for the development of biosensors and analytical devices: a review. *Anal Chim Acta* 872:7–25
43. Weblink 1: <https://www.healthline.com/health-news/new-study-found-80-percent-of-covid-19-patients-were-vitamin-d-deficient>
44. Weblink 2: <https://www.ncbi.nlm.nih.gov/pmc/articles/PMC7385774/>
45. Weblink 3: <https://jamanetwork.com/journals/jama/fullarticle/2775003>
46. Weblink 4: <https://www.nutraingredients.com/Article/2020/08/19/Study-adds-weight-to-link-between-COVID-19-and-vitamin-D>

Publisher's note Springer Nature remains neutral with regard to jurisdictional claims in published maps and institutional affiliations.